"Condensed Matter Theories"
(Nova Science Publishers, 1988)

TOWARDS A FIRST-PRINCIPLES DETERMINATION OF THE PHASE DIAGRAM OF C_{60}

J. M. Pacheco

Departamento de Física da Universidade
3000 Coimbra, Portugal

and

J. P. Prates Ramalho

Departamento de Química da Universidade
Apartado 97, 7001 Évora Codex, Portugal

1. INTRODUCTION

Buckminsterfullerene C_{60}, depicted in fig.1a, is a highly symmetric and stable molecule. Fullerenes are formed, for instance, when vaporised carbon condenses in an atmosphere of inert gas. The gaseous carbon is obtained e.g. by directing an intense pulse of laser light at a carbon surface. The released carbon atoms are mixed with a stream of helium gas and combine to form clusters of some few up to hundreds of atoms. The gas is then led into a vacuum chamber where it expands and is cooled to some degrees above absolute zero. Its discovery in 1985 [1] has generated a tremendous excitement and opened up a new field of carbon chemistry.

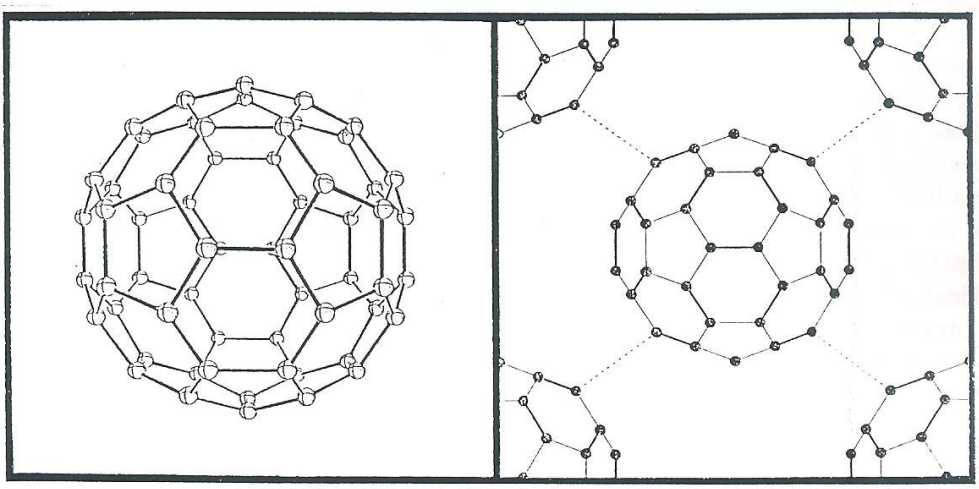

Figure 1. 1a. The Buckminster fullerene C_{60}. **1b**. Fullerite, the bulk form of C_{60}.

A decisive step which opened up the possibility to obtain most of the experimental information we have on fullerenes to date came up in 1990 [2], when the third stable form of carbon besides graphite and diamond, called fullerite, has been produced. It corresponds to a stable bulk material which has, as constituent units, the fullerene molecules. Fullerite has been obtained in isolable quantities by causing an arc between two graphite rods to burn in a helium atmosphere and extracting the carbon condensate so formed using an organic solvent.

The low-temperature structure of fullerite is identified to be cubic $Pa\bar{3}$ with the molecules orientationally ordered - see fig. 1b. At room temperatures, the C_{60} molecules undergo hindered rotation. As temperature or other thermodynamical variables are changed, fullerite undergoes several phase transitions, which are well-known and thoroughly studied - for a review, see ref.[3]. This is so except at temperatures above 1500 K. At such extreme conditions, the experimental methods are scarse and rather involved, precluding a detailed study. Theoretically, contradictory predictions have been advanced in the literature[4,5], in praticular in what concerns the existence or not of a stable liquid phase. This is unfortunate, since knowledge of the complete phase diagram of fullerite, besides its invaluable theoretical interest, may prove relevant for the optimization of its purification process.

In refs.[4,5], computer simulations have been performed to study the different phase-coexistence lines, in order to answer the fundamental question of whether C_{60}-fullerite has a stable liquid phase. Both works made use of the classical Girifalco potential [6], arriving at contradictory results: While in ref. [4] no stable liquid phase would exist for fullerite - which would turn out to become the first pure substance to exhibit no triple point - in ref.[5] a marginally liquid phase was found to exist at atmospheric pressure around a temperature of 1800 K. The results, which start from the same input inter-fullerene interaction and make use of similar computational techniques, suggest that the high temperature behaviour fullerite may exhibit a remarkable sensitivity to the details of the inter-fullerene potential. In this context, it is questionable whether one should address such an important issue making use of a classical potential. Indeed, one can point out several undesirable features when using the Girifalco potential to compute the high-temperature phase-diagram of fullerite: Besides its intrinsic phenomenological nature, the inter-fullerene interaction is basically taken as a two-fullerene interaction only, in which each fullerene is usually treated as a superposition of non-interacting carbon atoms, therefore disregarding the individual character and high stability of the molecule as a whole. Furthermore, in such a framework, three-body terms are neglected, while it has been argued, on the basis of the large static polarizability displayed by the fullerene molecules, that these terms might provide a significant contribution [8]. Such features call for a better theoretical scheme to determine the inter-fullerene interaction. This is the purpose of the present work, in which an inter-fullerene interaction is worked out from first principles, not only its two-body part but also its dominant three-body term. This will be carried out in the Local Density Approximation (LDA) to Density Functional Theory (DFT) together with its extension for excited states, the Time-Dependent (TD) DFT [9]. It will be found that the interaction derived here leads systematically to a good and overall description of several properties of fullerite already determined experimentally. A comparison of our results with experimental data and with those obtained using the Girifalco potential puts in evidence the significant improvement

of the present inter-fullerene interaction with respect to the Girifalco potential in describing the high-temperature behaviour of fullerite, opening the way to provide an unambiguous answer in the quest for a stable liquid phase of fullerite.

After summarizing the theoretical framework utilized in this work in Section two, an analytical parametrization of the *ab-initio* data will be worked out in Section three, taking as an input the *ab-initio* results obtained here, together with those of ref. [10]. This analytic parametrization not only exhibits the right asymptotic behaviour of the inter-fullerene interation, but also provides the appropriate framework to carry out the computer simulations. These will be described in detail in Section four, where the main results will be presented as well. Section five will be devoted to the conclusions and future prospects. A summary of some of the main results presented here has been published elsewhere [11].

2. THEORY

The Local Density Approximation (LDA) for Exchange and Correlation (XC) in Density Functional Theory (DFT) has been shown to provide an accurate description of structural and electronic properties of a wide variety of materials, including the different stable forms of carbon [3,10]. This is so for structural situations in which the electronic densities of the interacting molecules overlap. Each carbon atom is often represented by means of a norm-conserving, transferable pseudopotential [12], leaving as active 4 valence electrons per atom. In this context, the calculation of ref. [10] typifies a state-of-the-art LDA calculation of fullerite, the results of which we shall utilize below. In such a framework, the ionic coordinates which specify the lattice arrangement of C_{60} molecules constitute the starting point of the calculation. For each lattice configuration, the total energy $E(\{\vec{R}_i\})$ is determined using an efficient algorithm based on iterative diagonalization to obtain the self-consistent solution of the Kohn-Sham equations. For the bulk forms of carbon, such a procedure is most efficiently implemented in a plane-wave-basis super-cell method, although its computational burden for the specific case of fullerite requires the use of a supercomputer. For the equilibrium configuration of fullerite, the nearest neighbour bond-lengths within each fullerene, as well as the inter-fullerene distance have been allowed to relax in order to minimize the total energy [10]. Subsequently, the total energy of fullerite has been computed in ref. [10] as a function of the inter-fullerene distance, for fixed carbon-carbon bond-lengths (see ref. [10] for details). Although one should, in principle, relax the carbon-carbon bond-lengths at each value of the inter-fullerene separation, such corrections would lead to total energy variations which have been estimated to amount to $\approx 7\%$. From the results of ref. [10] we shall extract the inter-fullerene interaction energy at small and intermediate distances. At large separations, we shall make use of the formalism described on the following.

As is well known, LDA-DFT is unable to describe correctly the long range behaviour of, e.g. the inter-fullerene interaction energy, which is dominated by dispersion interactions. This feature, which constitutes one of the major drawbacks of the theory, can be circumvented if we consider its linear response extension - TDLDA - for the description of excited states. Indeed, the long-range dispersion forces between fullerenes can be accurately calculated within TDLDA, once we compute the

polarizability tensor of one fullerene molecule, which constitutes the key ingredient [13] for the determination of the two-body van der Waals as well as the three-body Axilrod-Teller interactions, as can be seen from the following standard expression for the dispersion coefficients:

$$C_6 = \frac{3}{\pi}\int_0^{+\infty} {\alpha_d}^2(iE)dE \ , \tag{1}$$

$$C_8 = \frac{15}{\pi}\int_0^{+\infty} \alpha_d(iE)\alpha_q(iE)dE \ , \tag{2}$$

$$C_{AT} = \frac{3}{\pi}\int_0^{+\infty} {\alpha_d}^3(iE)dE \ , \tag{3}$$

In the expressions above, C_6 is the leading order van der Waals coefficient, C_8 is the second term in the van der Waals expansion of the interaction energy as a function of the inter-fullerene distance x,

$$W(x) = -\frac{C_6}{x^6} - \frac{C_8}{x^8} - \frac{C_{10}}{x^{10}} - \ldots \ , \tag{4}$$

whereas C_{AT} is the leading three-body dispersion term. All these three coefficients can be espressed in terms of the dipole polarizability $\alpha_d(iE)$ (C_6,C_{AT}) and the quadrupole polarizability $\alpha_q(iE)$ (C_8) tensors, computed at purely imaginary energies iE.

In keeping with this discussion, we computed the long-range interaction energy between two and three fullerenes via direct integration of eqs.(1-3), in which we employed the dipole and quadrupole polarizability tensors of C_{60} computed in TDLDA. The method we utilized extends to imaginary frequencies the linear-response method in coordinate space developed in ref. [14], which is well suited when applying the TDLDA to isolated molecules. In short, we start by solving the Kohn-Sham equations via the expansion of the solutions in a spherical basis, $\psi_k(\vec{r}) = \sum_{n\ell m} C^k_{n\ell m}\, \phi_{n\ell m}(\vec{r})$, where $\phi_{n\ell m}(\vec{r}) = R_{n\ell}(r)\, Y_{\ell,m}(\hat{r})$. We use the same pseudopotentials as those used in ref. [10], as well as the same XC functional. The functions $\phi_{n\ell m}(\vec{r})$ have been obtained by solving numerically the spherical part of the Kohn-Sham equations in a spherical box of 11.6 Å (22 a_0) of radius and using a mesh with a step of 0.01 Å. The coefficients $C^k_{n\ell m}$ of the expansion above have been obtained by including multipole moments of the ionic field up to $L = 20$ and all the spherical wave-functions with eigenenergies up to 40 eV. This means that spherical wave-functions having angular momenta in the range $0 \leq \ell \leq 20$ and number of nodes $n = 0, 1, 2, ..., 15$, have been considered. The energy gap between the highest-occupied and the lowest-unoccupied molecular orbital states (HOMO-LUMO gap) is predicted to have a value of 1.91 eV as compared to the value of 1.86 ± 0.1 eV measured experimentally [15]. The band width is predicted to be $\cong$ 21 eV, being controlled, to a large extent, by the non-local part of the pseudopotential. Making use of the single-particle basis discussed above, the dipole response of C_{60} has been worked out in the Time-Dependent Local

Density Approximation (TDLDA). The basic quantity to be calculated is the free density-density correlation function

$$\chi^{(0)}(\vec{r},\vec{r}\,';i\omega) = \sum_{ph} \Psi_{ph}(\vec{r}\,) g_{ph}(i\omega) \Psi^*_{ph}(\vec{r}\,') \quad , \tag{5}$$

where

$$g_{ph}(i\omega) = \left(\frac{1}{\Delta E_{ph} - i\hbar\omega} + \frac{1}{\Delta E_{ph} + i\hbar\omega} \right), \qquad \Delta E_{ph} = E_p - E_h$$

and

$$\Psi_{ph}(\vec{r}\,) = \psi^*_p(\vec{r}\,)\psi_h(\vec{r}\,) = \sum_{\lambda\mu} \Phi_{ph,\lambda\mu}(r) Y_{\lambda\mu}(\hat{r}).$$

The induced density within TDLDA corresponds to the self-consistent solution of the following equation,

$$\delta n(\vec{r}, i\omega\,) = \delta n^{(0)}(\vec{r}, i\omega\,) - \int d^3r_1 d^3r_2\; \chi^{(0)}(\vec{r},\vec{r}_1;i\omega)\; V(\vec{r}_1,\vec{r}_2\,)\; \delta n(\vec{r}_2, i\omega\,) \quad , \tag{6}$$

where

$$V(\vec{r}_1,\vec{r}_2\,) = 1/|\vec{r}_1 - \vec{r}_2\,| + \delta(\vec{r}_1 - \vec{r}_2\,)\; dV_{\rm xc}/dn \quad ,$$

and

$$\delta n^{(0)}(\vec{r}, i\omega\,) = -\int d^3r'\; \chi^{(0)}(\vec{r},\vec{r}\,';i\omega)\; M(\vec{r}\,) \, ,$$

with

$$M(\vec{r}\,) = e\sqrt{\frac{4\pi}{(2\lambda+1)}} r^\lambda Y_{\lambda 0}(\hat{r})$$

the multipole field, for which the values $\lambda = 1$ and $\lambda = 2$ correspond to dipole and quadrupole fields, respectively. Inserting in eq. (5) the multipole expansion of Ψ_{ph}, we can write

$$\chi^{(0)}(\vec{r}_1,\vec{r}_2;i\omega) = \sum_{\ell_a m_a, \ell_b m_b} \chi^{(0)}_{\ell_a m_a, \ell_b m_b}(r_1, r_2, i\omega)\; Y_{\ell_a m_a}(\hat{r}_1)\; Y_{\ell_b m_b}(\hat{r}_2) \quad , \tag{7}$$

where

$$\chi^{(0)}_{\ell_a m_a, \ell_b m_b}(r_1, r_2, i\omega) = \sum_{ph}\; \Phi_{ph,\ell_a m_a}(r_1)\; g_{ph}(i\omega)\; \Phi_{ph,\ell_b m_b}(r_2).$$

Expanding δn and V in spherical harmonics, the relation (6) transforms into a set of coupled linear equations in $r-$space. In the case of a dipole field,

$$\delta n_{10}(r, i\omega) = \delta n^{(0)}_{10}(r, i\omega) -$$

$$- \sum_{L'M'} \int dr_1 dr_2\, r_1^2 r_2^2\, \chi^{(0)}_{10,L'M'}(r, r_1; i\omega)\, V_{L'M'}(r_1, r_2)\, \delta n_{L'M'}(r_2, i\omega) \quad , \tag{8}$$

and similarly for the quadrupole case. These are the basic equations which we shall solve in the next section, and from which we shall extract the long-range behaviour of the inter-fullerene potential.

3. RESULTS AND PARAMETRIZATION

For each value of $i\omega$, we perform the Sum-Over-States in eq.(5) in order to compute the unscreened density-density correlation function $\chi^{(0)}$. This proves useful to check the convergence of this function which, in our case, is achieved by including $\approx 2 \times 10^4$ one-electron states in the calculation, corresponding to a cut-off at 40 eV. No approximations are introduced in the incorporation of screening, since we compute it self-consistently by solving the integral equation for the induced density, eq. (8), via a discretization of its multipole components in coordinate space. With this formulation we obtain, for the static linear polarizability of the fullerene molecule, a value of 90 $Å^3$, a value which has been recently corroborated, independently in ref. [16]. This value should be compared with the expected experimental value, which should fall in the interval 89-92 $Å^3$, obtained when one relates the static polarizability of the fullerene with the dielectric constant of fullerite via the Clausius-Mosotti relation [14]. In our calculations we utilized the same pseudopotentials [12] used in the plane-wave calculations of ref. [10], as well as the same XC functional, for which we took the Ceperley and Alder results [17] as parametrized by Perdew and Zunger [18]. We took advantage of the high (icosahedral) symmetry associated with the fullerene and computed the polarizability tensors with respect to the principal axes of the molecule in which both the dipole and quadrupole tensors are diagonal.

As expected [13], the polarizability is a smooth function of its purely imaginary argument, as one can judge from fig. 2, where the dipole and quadrupole polarizabilities are plotted as a funtion of the imaginary energy iE. Such a smooth behaviour makes it trivial to carry out the numerical integration of eqs. (1-3).

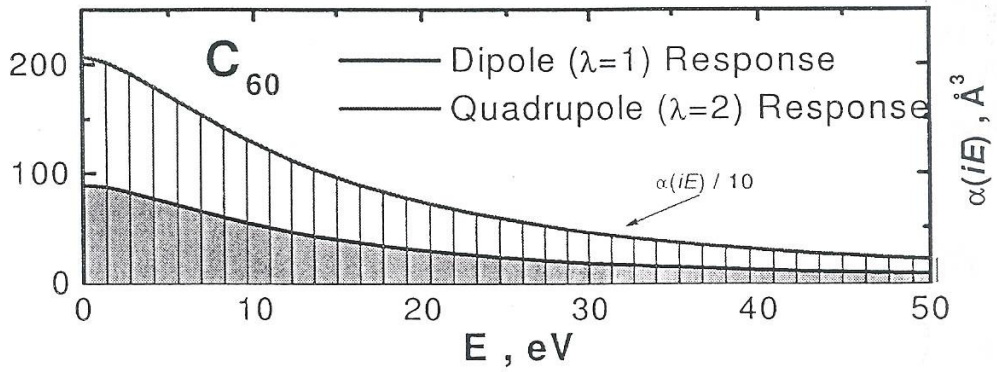

Figure 2. Linear dynamic dipole (shaded area) and quadrupole (dashed area) polarizabilities of fullerene C_{60} as a function of iE. The scale and units of the vertical axis in fig. 2 apply to the dipole polarizability. As indicated in the figure, the quadrupole data has been rescaled by one order of magnitude for direct comparison with the dipole polarizability.

Making use of the results displayed in fig. 2 we integrated eqs. (1-3) obtaining, for the dispersive two and three-body coefficients the results given in table 1 under the column FREE and TDLDA, in which we also compile results for the same quantities obtained at other levels of approximation. From table 1 one can judge the role of screening in the determination of the polarizability, which correctly brings the values of the (FREE)dispersion coefficients to the right orders of magnitude (TDLDA). Furthermore, one also concludes that the TDLDA results are very close to those obtained at other levels of approximation, at least in what concerns the C_6 van der Waals coefficient. On the other hand, only in the present calculation one has been able to compute, consistently with the 2-body terms, the 3-body dispersion coefficient C_{AT}.

Table 1	Girifalco	Girard	Bulgac	FREE	TDLDA
C_6 (eV Å^{-6})	20 N_{at}^2	17 N_{at}^2	15 N_{at}^2	144 N_{at}^2	21 N_{at}^2
C_8 (eV Å^{-8})	2520 N_{at}^2		2470 N_{at}^2	14709 N_{at}^2	2534 N_{at}^2
C_{AT} (eV Å^{-9})				580 N_{at}^3	22 N_{at}^3

Table 1 Values for the van der Waals coefficients C_6 and C_8, and for the Axilrod-Teller coefficient C_{AT} obtained using different levels of approximation (see main text for details). N_{at} is the number of atoms in a single fullerene (60). The values under the column Girifalco have been obtained by extracting the appropriate coefficients of the asymptotic expansion of the Girifalco potential. Those under the column Girard correspond to the semi-classical estimate of ref. [19], whereas those under Bulgac have been obtained integrating eq.(1) (transformed into the real-frequency domain by the usual dispersion relations) and utilizing for $\alpha(\omega)$ the values obtained in ref. [20] making use of a Tight-Binding formulation. The FREE results correspond to LDA results without inclusion of screening. Finally, in TDLDA the polarization of the electron cloud in the presence of an external field is included at the level of linear response. The values used in the production of the data plotted with solid squares in fig. 3 correspond to the results tabulated here under the column TDLDA.

Making use of the coefficients of table 1, and inserting their value into eq. (4), one can compute the long-range interaction energy between two fullerenes. This is plotted in fig. 3 with solid squares. Of course, in order to be able to parametrize the inter-fullerene interaction energy at all distances, one must complement the long-range calculation with consistent data obtained at intermediate and small distances. To this end, we make use of the results of ref. [10] in the way explained below, leading to the set of solid circles drawn in fig. 3.

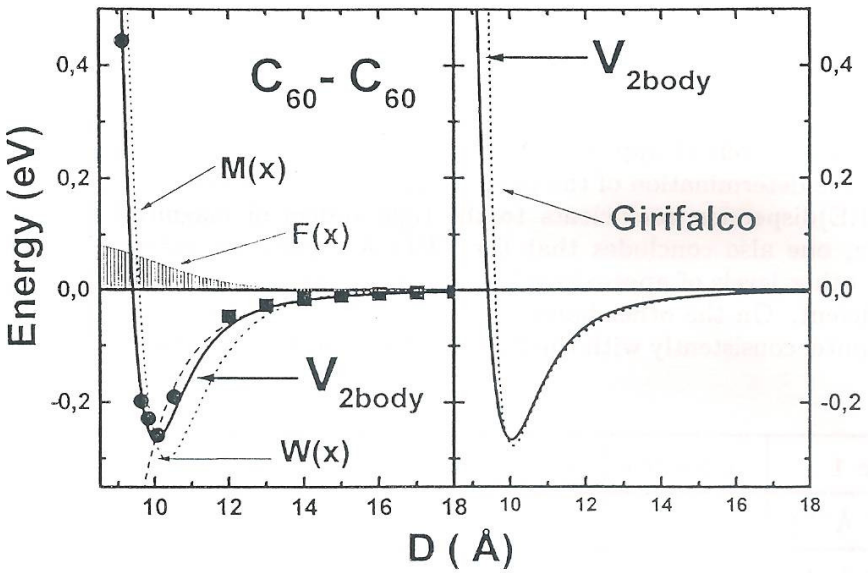

Figure 3. 3a Different contributions to $V_{2body}(x)$: The Morse potential $M(x)$ is drawn with a dotted line, and determines the exponential behaviour of $V_{2body}(x)$ at short distances. The long-range tail, represented by the van der Waals tail $W(x)$ is drawn with a dashed line. Finally, the crossover function of Fermi type F(x) delimits the dashed area and acts as a switch between the 2 limiting functions $M(x)$ and $W(x)$. $V_{2body}(x)$ is drawn with a solid line, following the same notation as in fig. 3a. The *ab-initio* data taken from ref. [10] are drawn with solid circles, whereas the long-range interaction energy computed here (see main text for details) is drawn with solid squares. The *ab-initio* data drawn have been used in the non-linear fit which resulted in $V_{2body}(x)$. **3b** Comparison of $V_{2body}(x)$ with the classical Girifalco potential used in most of the computer simulations carried out so-far.

In ref. [10] the cohesive energy of fullerite in an FCC primitive cell, as a function of the cell size parameter a, has been computed for small and intermediate inter-fullerene separations, at which there is still an overlap of the change densities. From the cohesive energy, we extracted the two-body interaction energy by assuming that the inter-fullerene interaction is pairwise additive, and takes place only between nearest neighbours. This seemingly crude assumption has been estimated in ref. [6] to lead to small errors. Indeed, the contribution from second and third nearest-neighbour interactions does not seem to exceed 4% which, in turn, makes our error fall within the level of accuracy one expects for our parametrization. The resulting data is displayed in fig. 3 with solid circles. In this way, we consistently computed the short distance repulsive potential, the long distance dispersive interaction, as well as we have obtained the potential behaviour near equilibrium. In fig. 3a, the dashed line corresponds to the Girifalco potential [6] used in most of the high-temperature Monte Carlo and/or Molecular dynamics simulations of fullerite, and which results from the superposition of atom-atom potentials of Lennard-Jones type. The solid line corresponds to the fit to the *ab-initio* data which we discuss on the following.

The *ab-initio* results clearly establish the asymptotic behaviours at short and long distances, evidencing a stiff repulsive wall at short distances together with the appropriate van der Waals tail. In order to parametrize this interaction we considered

two functions which display, individually, the expected limiting behaviour [21] of a two-body interaction at short and long distances: A Morse potential $M(x) = M_0 exp[\tau(1 - x/d_0)][exp[\tau(1 - x/d_0)] - 2]$ for the short range part [22], and a van der Waals expansion $W(x) = -C_6/x^6 - C_8/x^8 - C_{10}/x^{10} - C_{12}/x^{12}$ at long distances. The crossover of these two regimes has been obtained via a third function of Fermi type namely $F(x) = [1 + exp((x - \mu)/\delta)]^{-1}$. The final form of the potential reads, then

$$V_{2body}(x) = F(x) \times M(x) + [1 - F(x)] \times W(x)$$

In the non-linear fitting procedure, we varied freely the parameters μ,λ,M_0,τ,C_{10},C_{12}. The results obtained are given in table 2, whereas in fig. 3b we distinguish the relative role played by each of three functions which enter the final form of $V_{2body}(x)$. As can be seen from fig. 3 the quality of the fit is good, following the *ab-initio* data rather closely.

M_0 (eV)	τ	d_0 (Å)	C_{10} (eV Å^{-10})	C_{12} (eV Å^{-12})	μ (Å)	δ (Å)
0.3	9.75	10.3	$2.09 \cdot 10^8$	$7.78 \cdot 10^{10}$	10.05	1.04

Table 2 Values for the quantities defined in main text, obtained as a result of the non-linear fit of V_{2body} to the *ab-initio* data. The resulting interaction, V_{2body}, is plotted in fig. 3.

Moreover, $V_{2body}(x)$ is deeper than the pure van der Waals expansion (solid squares in fig. 1) as one approaches the region of overlap between the fullerene densities, in agreement with the general properties expected for this type of potential [21].

4. MONTE CARLO SIMULATIONS

In order to test the quality of our potential we have carried out several Monte Carlo (MC) simulations in a canonical ensemble. We computed the equilibrium pressure as a function of fullerite density, and we computed the equilibrium density of fullerite as well as the energy per particle at room temperature and at zero pressure. The simulations were performed at different densities for a 256 C_{60} molecule system, using the usual periodic boundary conditions and starting from a perfect FCC lattice. The intermolecular potential was truncated at 20 Å. For each simulation we let the system thermalize for 2000 MC steps. After this equilibration stage, 4000 MC steps were made to compute the thermal averages. Values of the equilibrium pressures calculated from the simulations for different densities are shown in fig. 4 compared with experimental data. The overall agreement is good for the whole range of pressures and puts in evidence the large compressibility of fullerite. The results displayed in fig. 4 with solid circles show that the trend observed experimentally (represented with solid squares and taken from ref. [23] is nicely reproduced with the present potential, in sharp contrast to the results obtained by performing the same

simulations using the Girifalco potential, displayed with solid triangles.

The good agreement obtained at high pressure is due to the relative softness of our potential compared with previous potentials including the Girifalco [6] and the 12-6 carbon-carbon interaction [24]. As these potentials consider rigid molecules, one could think that the use of a "soft" model for the molecule could be more effective at high pressures. Nevertheless, there are experimental [25] and theoretical [10] evidences that the C_{60} molecules are extremely resilient to pressure and the geometric structure of the molecule remains stable upon hydrostatic compression, at room temperatures, up to about 20 GPa, suggesting that the interaction is too complex to be well described by such classical site-site models.

For the equilibrium density and the cohesive energy of fullerite (per mole) at equilibrium density and zero pressure, we obtain 1.40 10^{21} cm^{-3} and 160.7 kJ/mol, respectively with V_{2body}, whereas experimentally one finds 1.44 10^{21} cm^{-3} and 167.9 kJ/mol, respectively.

Finally, we assessed the role of the Axilrod-Teller interaction in the determination of the same properties, for which we repeated the same simulations using not only $V_{2body}(x)$ but also the Axilrod-Teller term. We found essentially no changes as the equilibrium density or the density-pressure behaviour were concerned, but we found a 6% contribution to the cohesive energy. As usual, the role of these three-body terms is mostly repulsive, so we obtained an overall increase of 6% in the cohesive energy of fullerite. As pointed in ref. [8], the high static polarizability of fullerene C_{60} would *a-priori* suggest a contribution from the three-body dispersion terms larger than the 6% obtained here. However (and this is particularly clear if one uses the real-frequency expressions for the van der Waals coefficients) the charge density waves in the fullerenes occur at very high energies ($\approx$ 20 eV), a feature which acts to reduce the effective value of the dispersion coefficients, thereby determining the contribution obtained, which can be considered as a normal contribution.

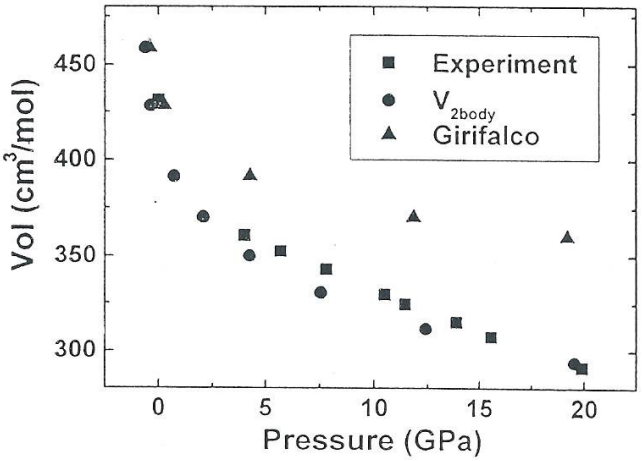

Figure 4. Molar volume of fullerite as a function of pressure. The solid squares display the experimental data taken from ref.[23]. The solid circles show the results of our Monte-Carlo simulations carried out with V_{2body} (see main text for details), whereas the solid triangles display the corresponding results when the simulations were carried out with the Girifalco potential.

5. SUMMARY AND OUTLOOK

We obtained a parametrized two-body inter-fullerene interaction derived from a parameter-free LDA calculation of the cohesive energy of fullerite, which exhibits a long-range behaviour governed by a dispersive inter-fullerene interaction computed consistently at the level of TDLDA. Furthermore, and making use of the same framework, we have computed the dominant contributions to the three-fullerene interaction via the calculation of the Axilrod-Teller coefficient C_{AT}. The major drawback of our method is the assumption that the fullerene-fullerene interaction in fullerite is pairwise and additive, thereby neglecting short-range n-body ($n > 2$) interactions. Although this effect has been argued to be small, it is included in an average way in our two-body interaction by means of our assumption, and therefore our interaction V_{2body} cannot be considered as a pure two-body term. Yet, this effective interaction has provided results which not only reproduce the trends observed experimentally, but also provide an overall agreement with experimental data which is good. Three-body dispersive interactions (not to be confused with the many-body correlations included in an average way before) are found to provide a repulsive contribution to the configurational energy of the order of 6%. This can be considered a "normal" contribution, in the sense that lies in the range which one usually obtains for van der Waals fluids. Yet, we believe that three-body terms may prove important in the quest for a stable liquid phase of C_{60}. Indeed, following the results of ref. [7], which make use of a Morse potentials, and performing a Morse fit to the *ab-initio* data, we obtain a potential which, again, is just on the borderline for meeting the criteria which ensures the existence of a stable liquid phase. Therefore, the three-body Axilrod-Teller interaction should not be overlooked when simulating the liquid-vapor and solid-vapor coexistence lines in fullerite. Work along these lines is in progress.

ACKNOWLEDGMENTS

We thank José Luís Martins for useful discussions, as well as for providing us the data for the inter-fullerene interaction at short distances. Financial support from PRAXIS XXI under contract PRAXIS / XXI / 2 / 2.1 / FIS / 473 / 94 is gratefully acknowledged.

REFERENCES

[1] H. W. Kroto, J. R. Heath, S. C. O'Brien, R. F. Curl, R. E. Smalley, Nature (London) **318** (1985) 162;

[2] N. Krätschmer, L. D. Lamb, K. Fostiropoulos, D. R. Huffman, Nature (London), **347** (1990) 354;

[3] M. S. Dresselhaus, G. Dresselhaus and P. C: Eklund, "Science of Fullerenes and Carbon Nanotubes", (Academic Press, 1995);

[4] M. H. Hagen, E. J. Meijer, G. C. A. M. Mooji, D. Frenkel, H. N. W. Lekkerkerker, Nature (London) ?? (1993) ??;

[5] A. Cheng, M. L. Klein, C. Caccamo, Phys. Rev. Lett. **71** (1993) 1200;

[6] L. A. Girifalco, J. Phys. Chem. **95** (1991) 5370; *ibid.*,**96** (1992) 858;

[7] J. P. K. Doye, D. J. Wales, J. of Phys. **B29** (1996) 4859;

[8] N. W. Ashcroft, Nature (London), **365** (1993) 387;

[9] A. Zangwill, P. Soven, Phys. Rev. **B21** (1980) 1561;

[10] N. Troullier, José Luís Martins, Phys. Rev. **B46** (1992) 1754;

[11] J. M. Pacheco, J. P. Prates Ramalho, Phys. Rev. Lett. (in press);

[12] N. Trouiller, José Luís Martins, Phys. Rev. **B43** (1991) 1993;

[13] G. D. Mahan, K. R. Subbaswamy, in "Local Density Theory of the Polarizability" (Plenum, N.Y., 1990), ch. 4;

[14] F. Alasia, H. E. Roman, R. A. Broglia, Ll. Serra, G. Colò, J. M. Pacheco, J. Phys. **B27** (1994) L643

[15] T. Rabenau et al., Z. Phys. B **90**, 69 (1993).

[16] S. J. A. van Gisbergen et al., Phys. Rev. Lett. **78** (1997) 3097;

[17] D. M. Ceperley, B. J. Alder, Phys. Rev. Lett. **45** (1980) 566;

[18] J. P. Perdew, A. Zunger, Phys. Rev. **B23** (1981) 5048;

[19] Ch. Girard, Ph. Lambin, A. Dereux, A. A. Lucas, Phys. Rev. **B49** (1994) 11425;

[20] A. Bulgac and N. Ju, Phys. Rev. **B46** (1992) 4297;

[21] Jacob N. Israelachvili, "Intermolecular and Surface Forces", Academic Press (London,1985);

[22] We would like to point out that a Morse fit alone is rather inefficient, due to its inability to provide accurate results at long distances. Such an approach has been exploited in ref [8] in connection to the Girifalco potential, where further details can be found.

[23] S. J. Duclos, Keith Brister, R. C. Haddon, A. R. Kortan, F. A. Thiel Nature (London), **351** (1991) 380;

[24] M. Sprik, A. Cheng, M. L. Klein, J. Phys. Chem. **96** (1992) 2027;

[25] M. Núñez-Regueiro, Mod. Phys. Lett. **B6** (1992) 1153;